

In-flight radiative decay and collision-induced ionization of N^{**}

H. U. Kiefl, H. Berst, and J. Fricke

*Physikalisches Institut der Universität Würzburg, Am Hubland,
8700 Würzburg, Federal Republic of Germany*

(Received 10 February 1982)

Highly excited fragments (N^{**}) from electron-impact dissociation of N_2 are studied in a time-of-flight technique. By using a sophisticated vacuum-ultraviolet filter technique we can show that more than 50% of the fragments in the atomic beam are Rydberg atoms belonging to the quartet system and more than 20% are doublet Rydberg atoms. We also succeeded in ending a controversy over the N^6S state: As it is not detectable in the metastable beam, its lifetime has to be considerably shorter than $10 \mu s$ because effective population of this state by electron impact seems to be very likely. From collisions of Rydberg atoms with several target gases, especially SF_6 , we learn that N^+ formation proceeds according to $\sigma \propto 1/v$ within the range 1–5 eV of collisional energies. We also give absolute cross sections for the N^{**} destruction by several electronegative gases.

I. INTRODUCTION

For many years highly excited atomic nitrogen (N^{**}) from electron-impact dissociation of molecular nitrogen has been a target of research. As far as the nature of the observed metastable species was concerned, somewhat controversial papers were published,^{1–5} interpreting N^{**} either as $6S$ nitrogen atoms or as Rydberg states or as a mixture of both (see Fig. 1). In the case of O_2 dissociation, the metastable O^5S state (9.14 eV above the ground state) is effectively populated, can be identified unequivocally, and studied in detail. Usually, time-of-flight (TOF) techniques are deployed to determine radiative lifetimes⁶ or cross sections for inelastic collisions.^{7–9}

With N_2 dissociation the situation is more complex. The metastable atomic N^6S state in question is located in the first continuum about 16 eV (Ref. 10) above the ground state and may decay optically or by autoionization. Early estimates of the $6S$ lifetime derived from measurements (there are no calculations) were of the order of $100 \mu s$.^{1–3,11}

In this work we can show that the N^6S state (1) is either too short-lived to be detected by our apparatus, i.e., $\tau < 10 \mu s$ (2) or it is not populated at all in electron-impact dissociation of N_2 and hence missing in the metastable beam. (This assumption seems to be rather unrealistic, as we will discuss later.) Furthermore, we demonstrated that (3) the detected metastable dissociation products are nitrogen Rydberg atoms which cascade down towards the ground state via certain intermediate levels, thereby emitting photons of characteristic wave-

lengths. The identification of the metastable dissociation fragments was possible by monitoring the faint characteristic emission lines of decaying beam particles in our TOF apparatus. This was done with the help of a special vacuum-ultraviolet (vuv) filter technique described earlier.^{7,8,12–14}

In addition, we studied collisional destruction of N^{**} atoms by electronegative gases. A distinct $1/v$ dependence of the cross section for this process occurs due to a purely attractive potential.

II. EXPERIMENTAL SETUP AND MEASUREMENTS

A schematic diagram of the apparatus used in these experiments is shown in Fig. 2. N^{**} meta-

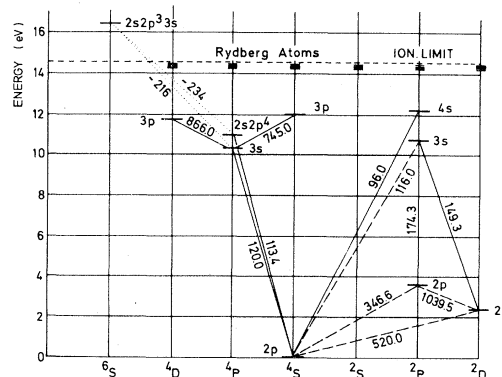


FIG. 1. Grotrian diagram of nitrogen. The $2s2p^3s$ $6S$ state in question lies roughly 2 eV above the first ionization limit and has to decay via 216- or 234-nm photons or it may autoionize.

SCHEMATIC OF APPARATUS

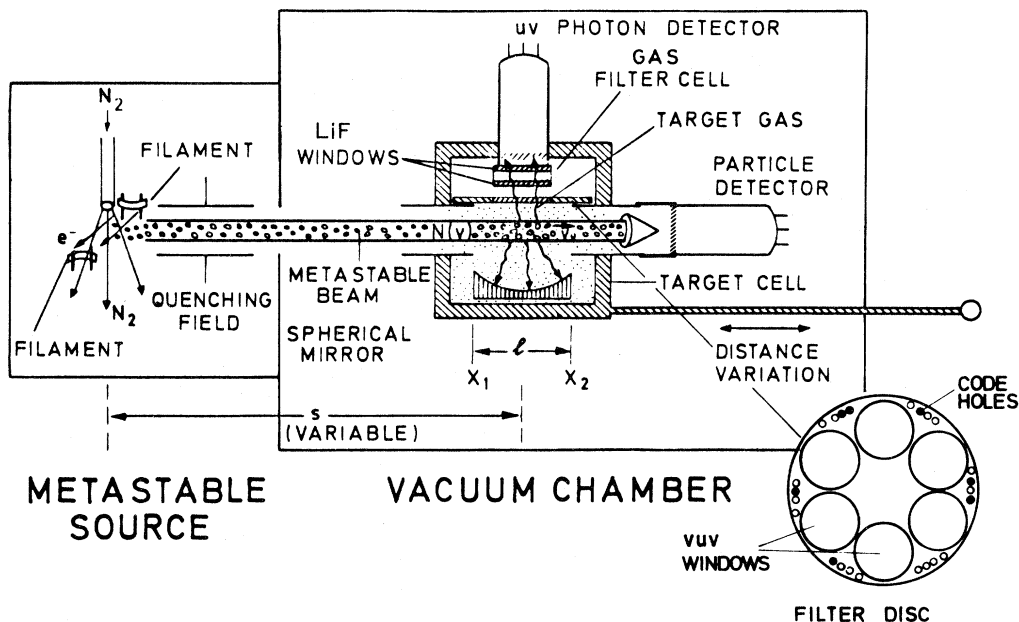


FIG. 2. Schematic of TOF apparatus with vuv photon detection system and particle detector. Photons from spontaneous decay of N^{**} are analyzed via a rotatable vuv filter disk and monitored by a closed photomultiplier. Particle counting is performed by an open multiplier via the Auger effect. The photon signal is enhanced by means of a spherical mirror. The viewing range of the photon detector is limited to $x_1 \dots x_2$. Gas is admitted into the target cell only for cross-section measurements.

stables were produced by electron-impact dissociation of N_2 with electron energies up to 130 eV. The metastables propagating in a direction perpendicular to both the N_2 and the electron beams passed a strong electric field of variable field strength from 10 kV/m up to 1200 kV/m. Thus charged particles were removed from the beam and atoms in high Rydberg states could be quenched. After collimation the metastables entered the main vacuum chamber containing the target cell with the detector assembly. While an axially mounted CuBeO multiplier monitored the beam via Auger electron emission by metastable impact (particle detector), a vertically positioned closed vacuum-ultraviolet photomultiplier (LiF window, BeO dynodes) registered photons from natural in-flight decay of metastables. As was shown previously,¹⁵ the secondary electron efficiency does not depend on the kinetic energy of the metastables at the energies involved. The optical viewing range covered about 1.5 cm of beam length. A rotatable filter disk was mounted between the photomultiplier and the atomic beam allowing six different vacuum-ultraviolet solid-state (mostly fluoride) windows to block the viewing

range of the multiplier. The filter positions could be selected and monitored from outside the vacuum chamber. The transmission behavior of the fluoride materials is shown in Fig. 3. The steep cutoffs in

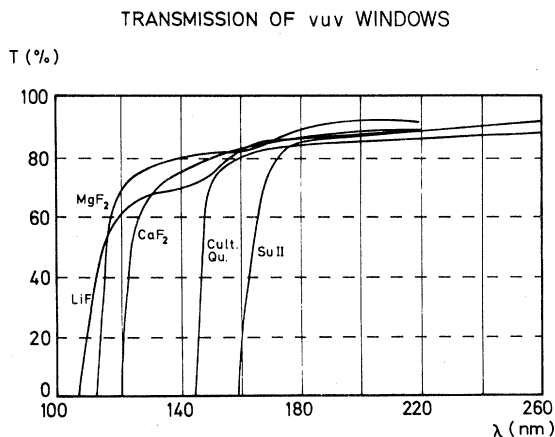


FIG. 3. Individual transmission curves for the vuv filters used in this work. The sharp cutoffs enabled us to effectively discriminate between the various atomic wavelengths (Su II is Suprasil II).

transmission allow nearly perfect discrimination between the photon wavelengths involved. Both the photon and the particle detector were rigidly mounted to the detector assembly. The distance between the detection unit as a whole and the metastable source could be varied by means of an external feedthrough.

Further details of the experimental setup, time-of-flight electronics, and the data acquisition system have been described elsewhere.^{9,12-14} The on-time of the electron gun was $2 \mu\text{s}$ in these measurements, while the TOF channel width was either 1 or $2 \mu\text{s}$. The TOF distance was 23, 31, and 46 cm, respectively.

III. RESULTS AND DISCUSSION

A. Comparison between particle and photon spectrum

Figure 4 shows two typical TOF spectra, one measured with the particle detector, the other taken with the photon multiplier. The count rate for the particle spectrum is roughly 100 times larger than

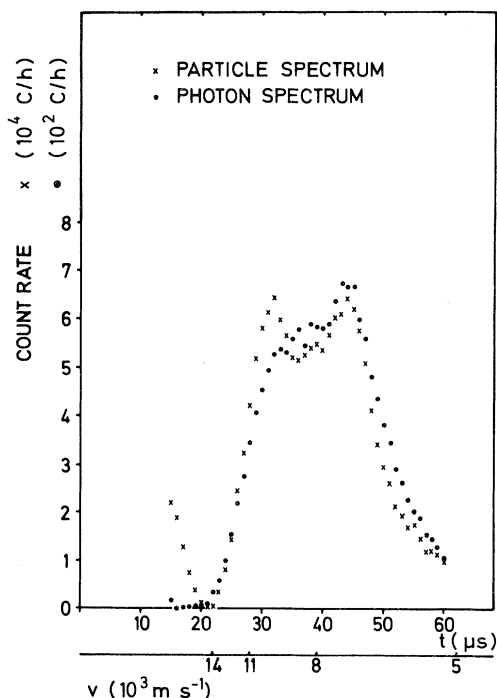


FIG. 4. Measured TOF spectra of N^{**} by particle and photon counting (MgF_2 window). Noise and counts from decaying molecules are suppressed. Each point coincides with a TOF channel, t is the time of flight and v the metastable velocity. The distance from source to detector was 31 cm in both cases.

that for the photon spectrum. Both, however, reveal the same structures, although with slightly different peak-height ratios and TOF channel resolution. These differences are solely related to the different detection procedures.

Let us first discuss the reason for the different peak-height ratios. The metastables decaying within the viewing range give rise to a count rate by the photomultiplier

$$R_{\text{opt}}(v) = CN_1(v)f[1 - \exp(-l/v\tau)] \\ \approx CN_1(v)fl/v\tau \text{ for } l/v\tau \ll 1, \quad (1)$$

where $N_1(v)$ is the number of metastables per pulse in the velocity range $v \cdots v + dv$ entering the viewing region, v the velocity of the metastables, τ an (average) lifetime of the metastables, f the electron pulse repetition rate, and l the length of the viewing region. The constant C takes care of the effective solid angle, the secondary electron yield of the multiplier, and the counting efficiency of the electronic amplification system.

As only a few percent of the metastables decay within the viewing range, the approximation made in Eq. (1) holds. In analogy the count rate from the particle multiplier is given by

$$R_{\text{par}}(v) = KN_1(v)f \quad (2)$$

with K taking into account the secondary electron yield and the counting efficiency of the particle detection system. By dividing (2) by (1) we get

$$R_{\text{par}}(v)/R_{\text{opt}}(v) = (K/C)v\tau/l \propto v. \quad (3)$$

By applying Eq. (3) to the TOF spectra in Fig. 4 the difference in peak-height ratios can be fully explained.

The TOF channel resolution of the two curves shown in Fig. 4 is slightly different. This is due to the relatively large viewing range of the photon detector of about 1.5 cm in contrast to the practically smooth surface of the particle detector. Especially the steep slopes of the photon TOF spectrum could be influenced by this effect. Point-by-point division of the measured spectra in Fig. 4, however, reveals a smooth slope confirming that both detectors actually register the same species of metastables.

B. The nondetectable N^6S state

Figure 5 shows spectra from radiative in-flight decay of the metastable N^{**} atoms for five different vuv windows as well as for no window at all. Taking into account the fluoride transmission

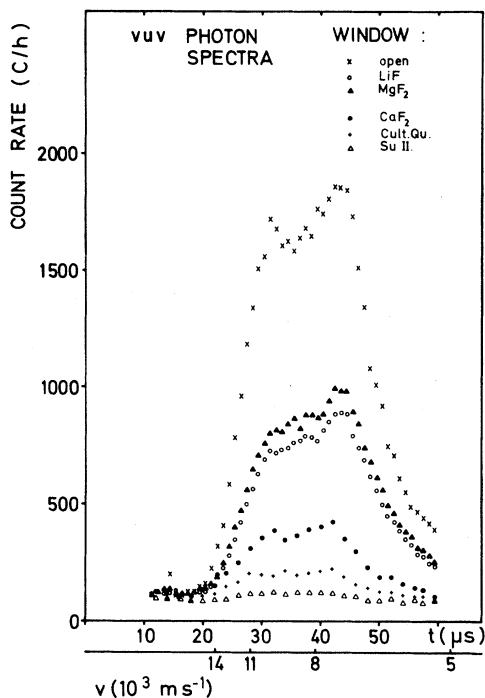


FIG. 5. Measured photon spectra of N^{**} with various vuv filter windows. The experimental conditions are the same as in Fig. 4. To extract information about the intensity ratios of the atomic lines involved, the transmission of the filter windows (Fig. 3) has to be taken into account.

curves (Fig. 3) it is obvious that most of the detected light occurs at wavelengths around 120 nm. Table I gives the measured intensities and wavelengths corresponding to the spectra of Fig. 5. Although the registered intensity drops drastically at longer wavelengths, i.e., with a CaF_2 window inserted, the basic TOF structure remains the same. From this fact we conclude that a large number of Rydberg states form the metastable beam. The argument against the presence of the N^{6S} state comes from the "core-ion model,"⁴ with each feature in the TOF spectra in this model being correlated to

another potential curve of the dissociating molecule. As both peaks in our spectra reveal practically the same intensity ratio at different wavelengths and in no case a strong reduction of one of the peaks, we have to conclude that the beam does consist of either Rydberg or N^{6S} atoms and not of a mixture of essentially different metastables. We preferred the Rydberg atoms because of the widespread wavelength range of the emission detected. This is contrary to several authors.¹⁻³ However, it is supported by work³⁻⁵ in which the authors correlated some of their TOF peaks with Rydberg atoms. (In Ref. 3 some peaks are interpreted as Rydberg atoms, others as N^{6S} atoms.)

Further information on whether the beam consists of N^{6S} atoms can be gained from a detailed analysis of the observed light intensities (Table I). N^{6S} has a $2s2p^33s$ configuration, a term energy of about 16 eV (ionization limit of 14.54 eV),^{10,16} and is the lowest-lying sextet state. While direct decay into the ground state is spin and parity forbidden, transitions via the $2s2p^4$ or the $2s^22p^23s$ configurations are only spin forbidden and should lead to photon emission of wavelengths 234 nm plus 113.4 nm or 216 nm plus 120.0 nm (see Fig. 1). However, neither the 113.4-nm nor the 234-nm and 216-nm transitions contribute (more than 2%) to the vuv photon spectra in Fig. 5, as can be derived from the LiF and MgF_2 curves and from the Suprasil-II curve at the very bottom (see Table I).

From the arguments given above we have to conclude that the detected metastables are Rydberg atoms and that the N^{6S} state has a lifetime against autoionization of below 10 μs . [Effective population of this state seems to be very likely as the electron energy (130 eV) in the metastable source is about five times larger than the threshold for production of the N^{6S} .]

It is remarkable that more than 50% of the in-flight decay light is concentrated around 120 nm. This light emission has to be correlated with the cascading down of Rydberg atoms within the quar-

TABLE I. Optical decay channels of the N^{**} -Rydberg atoms. (The wavelengths in parentheses are given in nm.)

| Wavelength/nm | Intensity/% | Transition |
|-----------------------------|-------------|---|
| $\lambda \leq 105$ | 26 | Higher states \rightarrow ground state |
| $105 \leq \lambda \leq 115$ | | No $2p^44P \rightarrow ^4S$ (113.4) |
| $115 \leq \lambda \leq 123$ | 54 | $3s^4P \rightarrow X$ (120.0); higher states $\rightarrow ^2P, ^2D$ (few %) |
| $123 \leq \lambda \leq 145$ | 12 | $4s \rightarrow ^2P$ (132.7); $3d \rightarrow ^2P$ (131-132); $3p \rightarrow ^2D$ (129) |
| $145 \leq \lambda \leq 160$ | 6 | $3s \rightarrow ^2D$ (149.3); $3p \rightarrow ^2P$ (147.1); $^4P \rightarrow ^2D$ (156.1) |
| $160 \leq \lambda$ | 2 | $3s \rightarrow ^2P$ (174.3); $^4P \rightarrow ^2P$ (183.7); [N^{6S} , 216, 234] |

tet system, towards the $4P$ state, and finally the 120-nm transition into the ground state. About 20% of the Rydberg atoms are certain to belong to the doublet system, as we would deduce from Table I by studying the emission lines between 123 and 160 nm.

We would like to point out that each of the decaying Rydberg atoms has to emit one vuv photon in order to bridge the 7-eV gap in the level diagram of nitrogen. It therefore has to appear in the vuv TOF spectra.

C. Rydberg atoms—lifetimes

After identifying the detected metastables as Rydberg atoms, we performed measurements to determine their lifetime (see Fig. 6). The TOF distances were 23 and 46 cm, respectively (see also Ref. 6). The data evaluation in this case was restricted to the 120-nm photons and to the TOF range shown in Fig. 5. Again it is demonstrated that the beam consists of a homogeneous mixture of Rydberg atoms (i.e., in each part of the TOF spectrum we

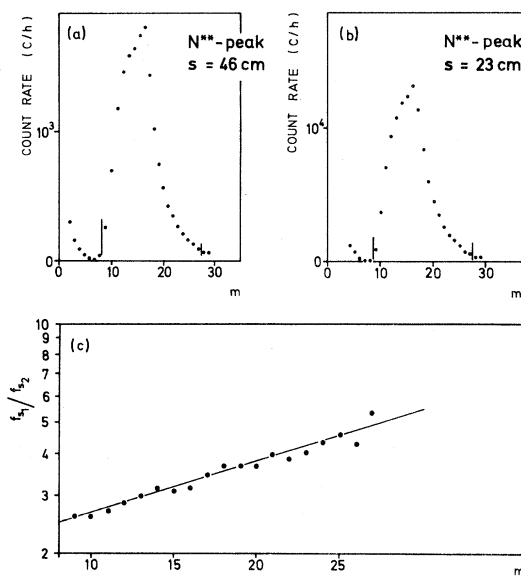


FIG. 6. TOF spectra with flight paths 23 and 46 cm are shown in (a) and (b), respectively. Both spectra are collected from mainly 120-nm photons (MgF_2 window) at an electric field strength of 10 kV/m. The intensity is given in counts per hour. The background is subtracted as in Figs. 4 and 5. m is the TOF channel number. The channel widths of both spectra are chosen according to the variation of the flight paths. The result of this division is shown in a logarithmic scale in part (c). The derived lifetimes vary between 60 and 30 μs for field strengths from 10 to 1200 kV/m.

have the same beam composition). For small electric quenching fields (10 kV/m), lifetimes around 60 μs result. Between 300 and 1200 kV/m (corresponding to a main quantum number $n=14$) the lifetime decreases slowly from 40 to 30 μs . This reduction is due to a successive quenching by field ionization of the long-lived Rydberg atoms with high quantum numbers. From $\tau \propto n^\beta$ with $\beta \approx 3.0-4.5$ (Refs. 17 and 18) and from $n_{max} \propto (1/E)^{1/4}$ (E = electric field strength; n_{max} = main quantum number of the highest surviving Rydberg states in an electric field),¹⁹ we would expect $\tau \propto E^{-\alpha}$ with $\alpha \approx 1-2$ by summing over n up to n_{max} . This behavior, however, is not observed, as a fast repopulation of Rydberg states is caused by the field gradient of the quenching barrier²⁰ and by interaction with the blackbody radiation of the vacuum chamber.²¹ Therefore, the beam composition changes only very little with field strength as does the lifetime.

However, the beam intensity is drastically changed by quenching fields¹⁹ (Fig. 7): Between 10 and 1200 kV/m the overall intensity decreases by a factor of 4. In addition—as can be seen—slower atoms are more effectively quenched than faster ones. This is due to the Stark effect, which reduces lifetimes against radiative decay as well as against autoionization by configuration mixing.¹⁹ As faster atoms stay in the field for a shorter time, they are more likely to escape.

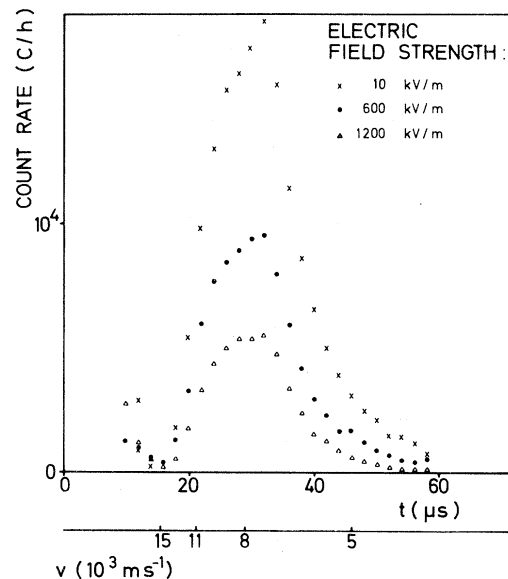


FIG. 7. Spectra for three different electric field strengths. The flight path is 23 cm. The reduction in beam intensity is due to electric field quenching.

D. Cross sections

To study inelastic collisions, the N^{**} beam was passed through gas admitted to the target cell (see Fig. 2). By comparing the TOF spectra with and without target gas, cross sections for the destruction of Rydberg atoms could be derived. Again we found that no N^6S atoms were present in the beam: The cross sections taken at quenching fields at 10 and 200 kV/m did not significantly change.

These measurements were performed with both the vertical and the axial detector. In the latter case the cross section is derived from the beam attenuation within the target cell:

$$R'_{\text{par}}(v) = R_{\text{par}}(v) \exp[-\sigma N(l+L)], \quad (4)$$

where R'_{par} is the counting rate with gas admitted, L the effective length of the cylindrical cell entrance and exit, l the length of the viewing region, and σ is the cross section for the extinction of metastables. The data evaluation in the case of the vertical detector was performed as follows:

$$R'_{\text{opt}}(v) = R_{\text{opt}}(v) \exp(-\sigma NL') \times \{ [1 - \exp(-\sigma NI)] / (\sigma NI) \}, \quad (5)$$

where L' is the effective length of the cylindrical cell entrance. The second exponential term takes into account that light is collected from everywhere within the viewing range and that the metastable intensity decreases with beam propagation.

In the first case [Eq. (4)], elastic scattering could contribute to the measured cross section, as particles may be scattered out of the detector solid angle. In the second case, however, elastic scattering cannot influence the count rate. Both results do agree within the error limit of absolute scaling (see caption of Fig. 8) and thus elastic scattering can be disregarded.

Figure 8 gives the cross section for ionization of N^{**} via the reaction

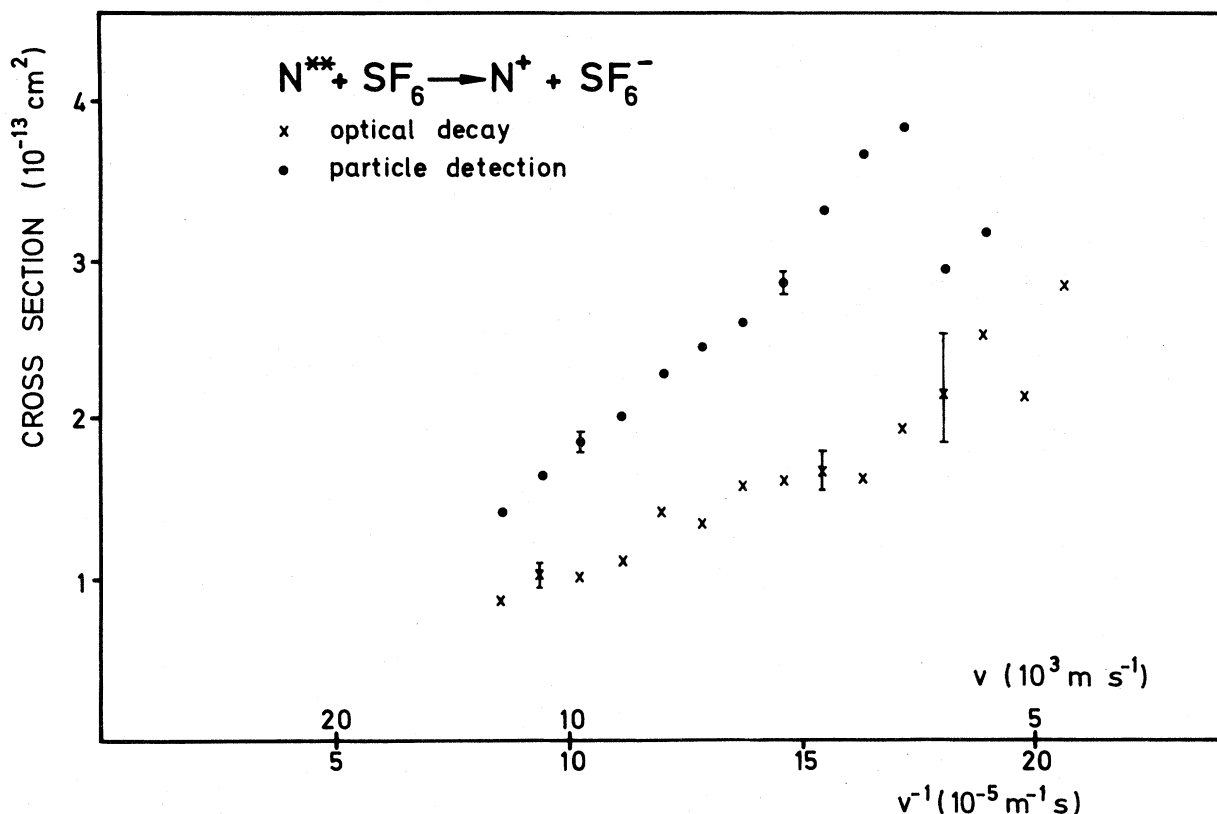
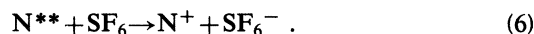


FIG. 8. Cross sections of N^{**} extinction by SF_6 as a function of projectile velocity. The error bars are solely due to statistical errors. The error for absolute scaling is about a factor of 2 and is due to uncertainties in the target-gas pressure and in the density variation of the gas along the beam path. This effect influences both measurements differently. The errors on the velocity scale are comparable to the distance between the data points.

TABLE II. Measured absolute cross sections of N** extinction by several target gases. The N** Rydberg states with $11 \leq n \leq 30$.

| Target gas | Electron affinity (eV) | Cross section $\sigma/10^{-15} \text{ cm}^2$ | |
|-------------------------------|------------------------|--|-------------------------|
| | | From decay-light detection | From particle detection |
| SF ₆ | ≈ 1.5 | 100–200 | 130–320 |
| C ₂ H ₂ | | 3– 6 | 2– 6 |
| C ₂ H ₄ | | 5– 10 | 5– 12 |
| C ₂ H ₆ | ≈ 1.5 | 9 | 5– 10 |
| O ₂ | 0.43 | 3 | 2– 4 |
| CO ₂ | 1.0 | 2– 4 | 2– 6 |
| N ₂ O | ≈ 1.0 | additional | 2– 3 |
| CF ₄ | 2.52 | light | 5– 15 |
| NO | 0.024 | production | 2– 4 |

Collisional deexcitation of N** to the ground state is very unlikely.²² The dominant exit channel is ionization of SF₆ by electron capture.²³ We see that σ is proportional to $1/v$ and rises up to $4 \times 10^{-13} \text{ cm}^2$ at the lowest available energies. For all other gases studied (Table II) σ is smaller by more than one order of magnitude. In most cases there again seems to be a $1/v$ dependence. To our knowledge, Fig. 8 shows the first cross-section measurements $\sigma = \sigma(v)$ for Rydberg atoms in the energy range 1–5 eV. Previous measurements were either made at thermal energies or in the keV range.²² SF₆ is generally well known for capturing free electrons,²³ as well as for ionizing Rydberg atoms very effectively.^{18,22}

The observed $1/v$ dependence can be attributed to an interaction with $\sigma \propto t_{\text{int}}$, where t_{int} is the duration of the “rendezvous.” Owing to the presence of the ionic core the Rydberg electron is smeared out over its orbit. Total cross sections for Rydberg collisions are given by Flannery²⁴ and Matsuzawa.²⁵ According to Flannery’s formula

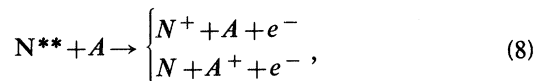
$$\sigma_{\text{tot}} = \langle v_e \sigma^T(v_e) \rangle / v, \quad (7)$$

where v_e is the electron (orbit) velocity, and σ^T the cross section for free electron scattering by the tar-

get molecule. The averaging has to be done over the velocity distribution of the electron’s atomic orbit. A rough estimate is possible by introducing a circular orbit for a certain n quantum number ($n=13$) and by using data from Ref. 26 for σ^T . The absolute values of σ_{tot} from Eq. (7) are about a factor of 3 larger than our results, while the v dependence does agree. Taking into account (i) the uncertainty of absolute scaling (see caption of Fig. 8), (ii) the fact that Flannery gives his cross section as an upper limit, and (iii) our rough estimate of σ_{tot} according to Eq. (7), the agreement is satisfactory. If one uses the electron attachment cross section for SF₆ given by Chutjian²⁷ instead of σ_T in Eq. (7) the reaction rate $\langle v_e \sigma_{\text{att}} \rangle$ can be shown to remain unchanged over the range of main quantum numbers $20 \leq n \leq 30$. The derived cross section σ_{tot} is then in good agreement (factor 1.5) with our data. A velocity-independent cross section, as it is assumed in Ref. 28, can be excluded for SF₆.

A threshold behavior in the formation of negative ions, as proposed for certain types of target gases²³ (not for SF₆, however, where the symmetry of ionic and neutral molecular state is the same and the bond lengths are only slightly different), could not be observed within the energy range of 1–5 eV.

Therefore, we conclude that (except for SF₆) the dominant inelastic process is the production of free electrons



where the cross section for this process seems to rise with increasing electron affinity (Table II).

ACKNOWLEDGMENT

We are indebted to Professor W. L. Borst for helpful discussions.

¹C. E. Johnson and H. A. Shugart (private communication).

²C. E. Fairchild, H. D. Garg, and C. E. Johnson, Phys. Rev. A **8**, 796 (1973).

³W. C. Wells, W. L. Borst, and E. C. Zipf, Phys. Rev. A **14**, 695 (1976).

⁴K. C. Smyth, J. A. Schiavone, and R. S. Freund, J. Chem. Phys. **59**, 5225 (1973).

⁵C. A. Kocher and C. E. Fairchild, J. Chem. Phys. **68**,

1884 (1978).

⁶G. Nowak, W. L. Borst, and J. Fricke, Phys. Rev. A **17**, 1921 (1978).

⁷H. U. Kiefl, W. L. Borst, and J. Fricke, Phys. Rev. A **21**, 518 (1980).

⁸H. U. Kiefl and J. Fricke, J. Phys. B **13**, 1185 (1980).

⁹J. Windrich, H. D. Wolf, and J. Fricke, J. Phys. B **11**, 1235 (1978).

¹⁰K. B. S. Eriksson, Phys. Scr. **9**, 151 (1974).

- ¹¹F. R. Innes and O. Oldenburg, *J. Chem. Phys. Lett.* **38**, 2306 (1963).
- ¹²H. D. Wolf, Diplom Thesis, Physikalisches Institut der Universität Würzburg, 1976 (unpublished).
- ¹³G. Nowak, Diplom Thesis, Physikalisches Institut der Universität Würzburg, 1977 (unpublished).
- ¹⁴H. U. Kiefl, Diplom Thesis, Physikalisches Institut der Universität Würzburg, 1978 (unpublished).
- ¹⁵W. L. Borst, G. Nowak, and J. Fricke, *Phys. Rev. A* **17**, 838 (1978).
- ¹⁶A. B. Prag and K. C. Clark, *J. Chem. Phys.* **39**, 799 (1963).
- ¹⁷H. A. Bethe and E. A. Salpeter, *Quantum Mechanics of One- and Two-Electron Atoms* (Academic, New York, 1957), p. 269.
- ¹⁸R. F. Stebbings, *Science* **193**, 537 (1976).
- ¹⁹M. G. Littmann, M. M. Kash, and D. Kleppner, *Phys. Rev. Lett.* **41**, 103 (1978).
- ²⁰M. L. Zimmermann, M. G. Littmann, M. M. Kash, and D. Kleppner, *Phys. Rev. A* **20**, 2251 (1979).
- ²¹W. E. Cooke and T. F. Gallagher, *Phys. Rev. A* **21**, 588 (1980).
- ²²R. F. Stebbings, *Adv. At. Mol. Phys.* **15**, 77 (1979).
- ²³H. Massey, *Negative Ions* (Cambridge University Press, London, 1976).
- ²⁴M. R. Flannery, *Phys. Rev. A* **22**, 2408 (1980).
- ²⁵M. Matsuzawa, *J. Phys. Soc. Jpn.* **32**, 1088 (1972).
- ²⁶J. Ferch, C. Masche, and W. Raith, *Abstr. Eur. Conf. At. Phys.* **5AII**, 698 (1981).
- ²⁷A. Chutjian, *Phys. Rev. Lett.* **46**, 1511 (1981).
- ²⁸M. Matsuzawa, *J. Phys. B* **8**, 2114 (1975).